




Growth kinetics and structure of a colloidal silica-based network: in situ RheoSAXS investigations

Konstane Kvaem Seljelid^{1,a} , Osvaldo Trigueiro Neto^{1,b}, Andrew Ndubuisi Akanno^{1,c}, Bruno Telli Ceccato^{1,d}, Rini Padinjakkara Ravindranathan^{1,2,e}, Namrah Azmi^{1,f}, Leide P. Cavalcanti^{3,g}, Ingebret Fjelde^{4,h}, Kenneth Dahl Knudsen^{1,2,i}, and Jon Otto Fossum^{1,j}

¹ Department of Physics, Norwegian University of Science and Technology, Trondheim 7491, Norway

² Institute for Energy Technology, IFE, Kjeller 2027, Norway

³ ISIS Neutron and Muon Source, STFC, Didcot OX11 0QX, UK

⁴ Norwegian Research Centre AS, NORCE, Stavanger 4021, Norway

Received 3 March 2024 / Accepted 8 July 2024

© The Author(s) 2024

Abstract Silica gels have a multitude of applications ranging from cosmetics and food science to oil and gas recovery. For proper design and application, it is important to have a thorough understanding of the underlying mechanisms of gel formation under different circumstances. The growth and structure of colloidal silica gels has been investigated using RheoSAXS to study the effect of silica concentration, NaCl concentration, temperature and shear rate. Additionally, SAXS in combination with a strong magnetic field has been applied to investigate the effect of magnetic microparticles and magnetic field on the development of the gel structure. Results indicate that the strongest effect on the gel kinetics are achieved by altering the activator concentration, here in the form of NaCl, followed by silica concentration and temperature. Small structural effects were also observed, with larger cluster sizes being produced at lower silica concentration and at higher NaCl concentration. Applying shear caused major changes both in structure as well as the macroscopic behavior of the silica, preventing the gel from reaching an arrested state, instead forming a viscous liquid. Applying a magnetic field appears to suppress the formation of larger clusters. The same effect is observed for increasing magnetic microparticle concentrations.

1 Introduction

Silicon is the second most abundant element in the earth's crust and its complex with oxygen producing silica, SiO₂, is the primary constituent of most rocks, and makes up around 60% of the earth's crust [1]. For this reason silica has been important in many different application throughout history. Everything from weapons, pottery, building materials and glass contain significant portions of silica in one form or another. In modern times silica in its more pure form continues to be of vital importance in many industries. Glass, semiconductor technology, cosmetics, oil and gas industry and medicine are some of the areas in which silica is being utilized.

A specific form of silica, known as silica gels have been widely studied due to their unique properties [2–9]. They have been used as adsorbents for water vapor [10], and are being investigated as potential good candidates for biogas adsorbents [11]. In addition to this, such silica gel materials could be used in combination with other

^a e-mail: konstane.k.seljelid@ntnu.no (corresponding author)

^b e-mail: osvaldo.t.neto@ntnu.no

^c e-mail: andrew.akanno@ntnu.no

^d e-mail: bruno.t.ceccato@ntnu.no

^e e-mail: rini@ife.no

^f e-mail: namrah.azmi@ntnu.no

^g e-mail: leide.cavalcanti@stfc.ac.uk

^h e-mail: infj@norceresearch.no

ⁱ e-mail: kenneth.knudsen@ife.no

^j e-mail: jon.fossum@ntnu.no

materials as a scaffolding material for bone tissue engineering [12, 13]. Silica gels have also found their use in the oil and gas industry, where they are being tested as a more environmentally friendly alternative to polymer gels which have been used for conformance control in reservoirs [14].

Colloidal silica dispersion for conformance control are studied utilizing rheological methods primarily. Metin et al. [15] studied two different types of colloidal silica gels using a rheometer to characterize the storage and loss modulus. They found that the gel time was highly dependent on the silica concentration, salt concentration and temperature. However, the critical strain was found to be independent of the silica concentration. Similar results were also found by Hatzignatiou et al. [16], Pham and Hatzignatiou [17].

Others have studied colloidal silica from a nano- and microscale perspective through various scattering techniques such as dynamic light scattering, as well as small angle X-ray and neutron scattering. Johnsson et al. [18, 19] used time resolved small angle X-ray scattering together with electro-spraying combined with a scanning mobility particle sizer, to investigate the effect of primary particles on final morphology of the silica gel network, as well as the effect of gel initiator type. From this study they found that with monodisperse and spherical primary particles, the aggregates formed dimers and trimers and subsequently more compact spherical aggregates. Introducing sample polydispersity caused larger aggregates to form at an earlier stage, however the final clusters remained spherical in shape. In contrast, gelling a solution of preaggregated spherical silica particles produced more end-to-end contacts and produced final gel networks that were more open, with elongated aggregates. In terms of activator, it was found that the aggregates and the obtained gel morphologies were not affected by the type of activator, however the rate of stability increase after the point of gelation was raised by the presence of strongly hydrated counterions.

The demands on the properties of silica gels vary depending on the final application of the system. To be able to design products performing within specific boundaries it is becoming increasingly important to know the relation between nano/microscopic properties and the resulting macroscopic properties. Previous studies of colloidal silica are for the most part focused on either the macroscopic or the microscopic aspect of the colloidal gel. Here we combine these two approaches to study a colloidal silica gel using the combination of small angle X-ray scattering and rheology. We have investigated how silica concentration, NaCl concentration, temperature and shear, as well as magnetic microparticles and magnetic field, affect the structure of the gel network at the nanoscale and the macroscopic rheological properties. We believe these results to be valuable for a better understanding of the dynamics of gel formation as well as for control of silica gel formation in practical applications.

2 Experimental method

Experiments were performed at Diamond Light Source (DLS) on beamline I22 and at the European Synchrotron Radiation Facility at beamline BM26. At I22 simultaneous Small angle X-ray Scattering (SAXS) and in situ rheology measurements, also called RheoSAXS, were performed, while at BM26 only SAXS was performed.

2.1 Materials

For all experiments a sodium stabilized silica dispersion, Levasil OF50 P from Nouryon, containing 15 wt% amorphous SiO₂ nanoparticles (5 nm in diameter) was used. The pH range of the solution ranged between 9.7–10.5, as given from the supplier. The Zeta-potential of the silica stock solution without any salt addition was measured with the instrument Malvern NANOZS. The Zeta-potential was (-48 ± 3) mV at 25°C, indicating good stability of the dispersion. A 2 M NaCl solution was prepared to be used as an activator for samples measured at I22. For the measurements at BM26 a stock solution of 2.6 M NaCl was used. For the pre-tests with CaCl₂ stock solutions, 0.5 M and 0.25 M were tested.

2.2 Pre-selection

In order to find a suitable range of gel times, a variety of silica concentrations and salt concentration were initially tested using the bottle method. The gel time aimed for was roughly an hour at room temperature, for practical reasons. Various amounts of silica and salt solutions (NaCl, CaCl₂) were mixed in small bottles and left to create a gel. On regular intervals the bottles were checked for gelling by tilting them slightly. The gel time was determined as the time at which the bottle could be turned up-side down without any sliding of the gel, as shown in Fig. 1. Salt solutions containing Ca²⁺ ions gelled immediately upon contact with these solution even at very low concentrations, as demonstrated in Fig. 2. After determining a rough range of gel times using the bottle method, the samples with a gel time close to one hour were measured on an Anton Paar MCR 301 rheometer with a Couette cell using oscillation mode to record the storage and loss modulus. These measurements, as shown in Fig. 3 were used to determine the gel time more precisely, defined as the crossover where the storage modulus exceeds the loss modulus, denoted in the figure with a vertical black line.

Fig. 1 Two gelled samples according to the bottle test method



Fig. 2 Bottle test with CaCl_2 and varying amounts of silica. The vol% here refers only to the volume of added Levasil OF50 P dispersion, not the volume percent of the colloidal silica

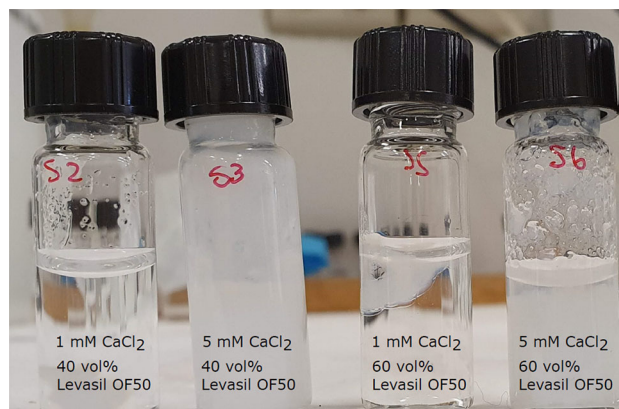
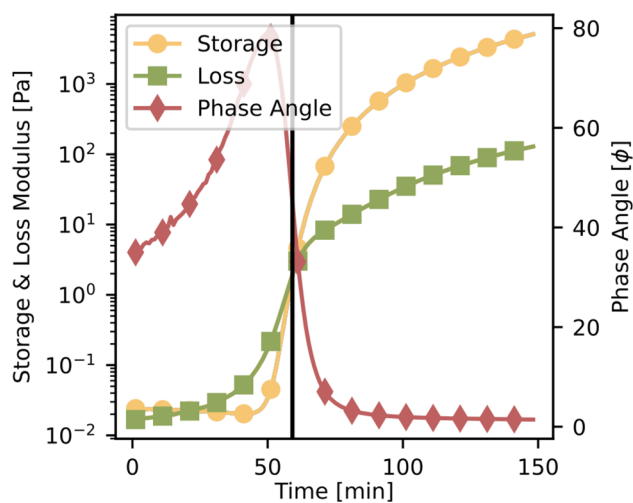


Fig. 3 Gel time determination from storage and loss modulus on a test sample. Black vertical line denotes the gel time



2.3 I22—sample preparation

Samples of different concentrations were prepared by adding different volumes of distilled water, Levasil OF50 P and 2 M NaCl solution, respectively, to a beaker, and mixing with a magnetic stirrer for 1 min. Sample solution (6 mL) was then transferred with a pipette to the rheometer measuring cup. Measurements of the samples at 20°C started 10 min after addition of the NaCl solution, without pre-shearing them. For samples measured at 40°C, it was only 5 min between NaCl addition and start of measurement.

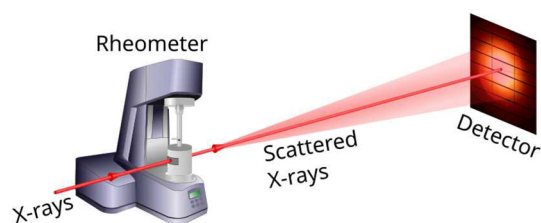
2.4 I22 rheometry

An Anton Paar MCR 501 rheometer with a polycarbonate measuring cell (ME/PC49) was used with the beam passing through the center of the cup. A solvent trap was used to prevent evaporation during experiments. Three types of measurements were performed using the rheometer. Oscillation with a strain (γ) of 5 % and an angular frequency (ω) of 10s^{-1} was used to measure the storage and loss modulus as well as the shear stress. From this the complex viscosity was calculated and used to estimate the gel time. The oscillation measurements were not considered to disrupt the system significantly as they were performed within the linear viscoelastic range [20], and we thus assume that the gelling proceeds near similarly to a sample measured without any external influences, e.g. a non-sheared sample. In contrast, for some samples a constantly applied shear rate was used to investigate the effect of shear on the gelling process. Shear rates between 1s^{-1} to 1000s^{-1} were applied. For all measurements each measurement point was measured for 60 s and the temperature was controlled by a Peltier element.

2.5 I22 SAXS setup

A simplified sketch of the experimental setup at I22 can be seen in Fig. 4. A monochromatic beam of wavelength of 0.100 nm was chosen in combination with the longest achievable sample to detector distance (9.864 m) in order to reach a typical q -range from $2.5 \cdot 10^{-2}\text{nm}^{-1}$ to 1.2nm^{-1} . A 2D Pilatus P3-2 M detector was used for data collection and the data were reduced using the Dawn Science software [21, 22]. A measurement of the sample cell with distilled water was used as a background measurement and subtracted from the signal.

Fig. 4 RheoSAXS experimental setup at I22



2.6 Sample preparation BM26

A similar approach to the one used at I22 was used at BM26, however with some small modifications. Samples were prepared in 2 ml Eppendorf tubes, where the distilled water, Levasil OF50 P, magnetic Dynabeads and lastly 2 M NaCl solution was added. Magnetic Dynabeads are monodisperse spherical polystyrene microbeads with an iron core that are superparamagnetic. Dynabeads are widely used in bio-molecular separation. The Eppendorf tube was closed and shaken with a vortex mixer for 1 min. Subsequently the solution was transferred from the tube to a 2 mm Hilgenberg glass capillary using a syringe. Lastly the capillary was sealed with UV glue and placed in the sample holder for measurement.

2.7 Sample holder at BM26

Figure 5 shows the custom made sample holder for the experiments at BM26. The sample holder consisted of a small aluminum piece with a slot for the capillary to enter and a hole where the X-ray beam would hit. The capillary was covered inside the aluminum block, except for the portion inside the opening made for the x-ray beam. The aluminum piece was connected to a circulating cooler, maintaining the temperature at 20°C .

Fig. 5 Sketch: custom sample holder used at BM26



2.8 BM26 SAXS setup

Similarly to the setup at I22, a monochromatic beam of wavelength 0.103 nm was used in combination with a sample to detector distance of 9.342 m. The detector was a 2D Pilatus 1 M, and the collected data were reduced using the Bubble software [23]. For background subtraction a capillary of pure water was measured and subtracted from the signal.

At the sample position an electromagnet was placed for controlling the magnetic field that the sample would be exposed to. The magnet was a 4T superconducting magnet borrowed from the XMaS beamline at the ESRF [24]. The magnet was placed so that the magnetic field was applied vertically, perpendicular to the X-ray beam.

2.9 Data modeling

Small angle X-ray scattering curves from systems of aggregating units are generally described by a Guinier region, followed by a power-law region. In 1995 G. Beaucage published a model which combines the contributions from the two regions into a unified scattering curve, allowing for fitting of small angle scattering data over multiple decades of the scattering vector, q [25]. The Beaucage unified model has since been widely used for describing various systems of aggregating particles [26–30].

The Guinier region provides information regarding the primary particle and aggregate sizes through the radius of gyration. The power-law on the other hand relates the slope of the linear region of the scattering curve to the fractal dimension. The fractal dimension can tell us whether a system can be considered as a mass fractal or a surface fractal. If the exponent of the power-law region is smaller than 3, it can be considered a mass fractal, while if the exponent lies between 3 and 4 it is a surface fractal [31]. For a mass-fractal system the fractal dimension gives a measure of how densely particles are packed, while for a surface fractal it is a description of the surface roughness. The unified model put forward by Beaucage is given in Eq. (1),

$$I(q) = C + S \sum_{i=1}^N \left[G_i \exp\left(-\frac{q^2 R_{gi}^2}{3}\right) + B_i \exp\left(-\frac{q^2 R_{g(i+1)}^2}{3}\right) \left(\frac{1}{q_i^*}\right)^{\alpha_i} \right], \quad (1)$$

where

$$q_i^* = q \left[\operatorname{erf}\left(\frac{q R_{gi}}{\sqrt{6}}\right) \right]^{-3}$$

$I(q)$ is the scattering intensity, C is a value related to the background scattering, S is a scaling factor, G_i is the Guinier scaling factor, q is the scattering vector, R_{gi} is the radius of gyration, B_i is the power-law scaling factor, α is the fractal dimension, and q_i^* is given above, where erf is the error function.

This model can be expanded for multiple Guinier and power-law regions, by adding another level, e.g. increasing N from 1 to 2. The model is available in the software *SasView* [32], and this was used to fit our data with a two-level model. Initial values for R_{g1} , R_{g2} , α_1 and α_2 were set to 3.6 nm, 10 nm, 3 and 1.40, respectively. The resulting parameters from the fit can be found in Table S1 and S2 in the Online Resource. The data were fitted in the q -range $0.025 \text{ nm}^{-1} < q < 0.95 \text{ nm}^{-1}$, and the fit for one of the samples is shown in Fig. 6. The model does not manage to capture the upturn in intensity at the lowest q values. This could have been accounted for by adding another power law term in the model. However, this was not implemented as the data in the low- q region that this would be interesting for is limited.

Multiple configurations of the fitting parameters were tested. For the primary particle the radius of gyration and power-law exponents were kept constant, and different variations of keeping G_1 and B_1 constant, letting one or both vary were tested. It was found that only minor differences were produced by the different configurations. Thus, the final fitting was performed keeping all parameters of the primary particle constant, except G_1 .

3 Results and discussion

Viscosity data were collected to extract the gelling time for the various sample compositions, cf. Figure 7 that will be discussed more later. Small Angle X-ray Scattering (SAXS) patterns were recorded and reduced to scattering curves for samples of varying silica concentration, NaCl concentration, temperature and applied shear. Figure 8 displays the results for samples of 9 and 12 wt% SiO_2 . We use the 12 wt% sample with 325 mM NaCl at 20°C and without shear (NS) (green curves) as a reference to which all the other data are compared when each parameter is changed. The cutoff for each sample at high q is due to the edge of the detector. Note that all data presented

Fig. 6 Model fit for one of the curves of the sample 12 wt% SiO₂, 325 mM NaCl, 20°C and no shear

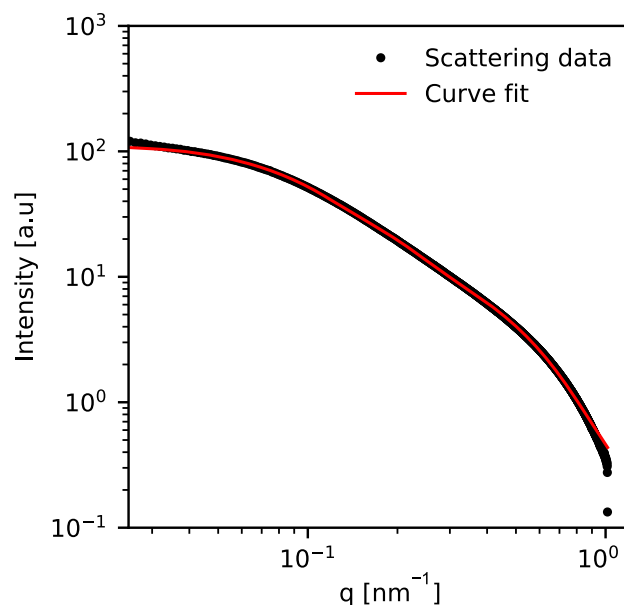
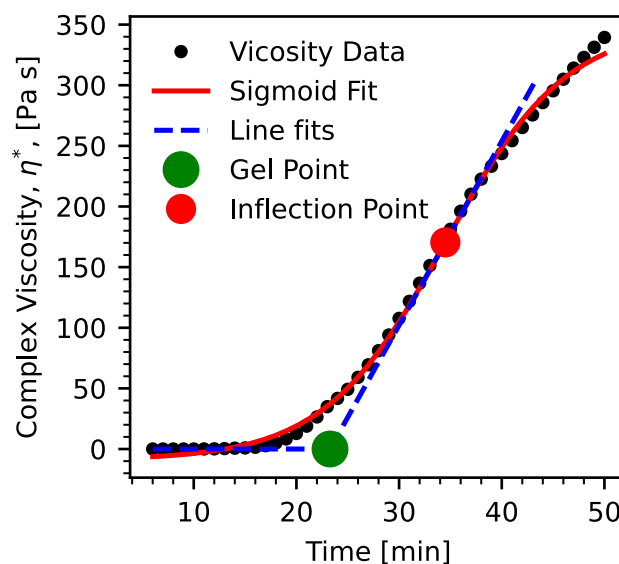


Fig. 7 Determination of gel time from viscosity curve. Inflection point determined from the sigmoid fit (red curve) of the viscosity data (black points). Gel point (green point) determined as the intersection of two linear fits (blue dashed lines) of the two different regions of the viscosity plot



have been normalized to the particle concentration to remove simple effects such as vertical scaling of the pattern due to change in silica concentration. This allows to better isolate effects that are related to internal restructuring in the system.

3.1 Silica concentration

From Fig. 8a, it can be seen that reducing the silica concentration to 9 wt% did not initially cause any major changes. The curves of the 12 wt% and 9 wt% samples overlap nearly perfectly in the beginning, showing that the internal structure is similar at $t=0$. The 12 wt% sample shows initially a slightly larger spacing between the curves, indicating that the structure is developing more rapidly than for the 9 wt% system. As time passes, the space between curves reduces for both samples due to the gel formation. The network formation locks the structure more in place, and thus the changes in the structure are occurring at a slower rate.

Fitting the scattering curves with the Beaucage Unified Model also demonstrates the similarities between the curves. Figures 9 and 10 show the development of the radius of gyration for the aggregates, which here will be referred to as the cluster size, and the fractal dimension of the systems, respectively. Comparing 9 wt% and 12 wt% SiO₂ the cluster sizes of the 12 wt% are initially growing slightly faster (Fig. 9a). This holds up until roughly 70 min, where there is a crossover as the growth rate of the clusters for the higher silica concentration is

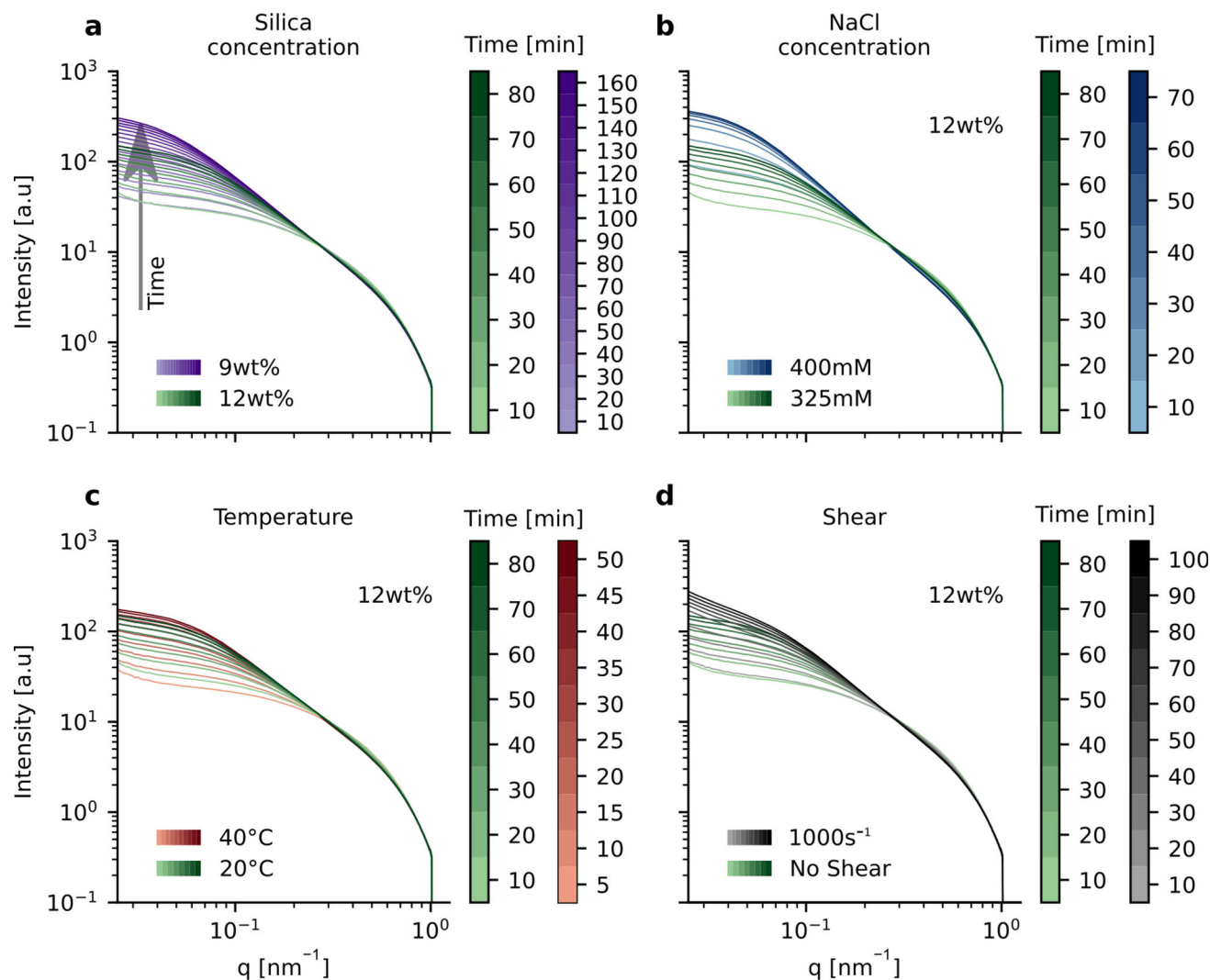


Fig. 8 Scattering intensity, I , as a function of scattering vector q . Each curve represents a different moment in time, marked by the different colors. **a** Comparison of two different silica concentrations, 9 wt% and 12 wt% with a NaCl concentration of 325 mM, temperature at 20°C and no shear applied. The black arrow shows the direction of time (same for **b**, **c**, **d** as well.) **b** NaCl concentration comparison for samples of 12 wt% silica, at 20°C and with no shear applied. **c** Temperature comparison for samples of 12 wt% silica, 325 mM NaCl with no shear applied. **d** Shear comparison for samples of 12 wt% silica, 325 mM NaCl at 20°C. All data have been normalized to the silica particle concentration

Table 1 Gel times for the different samples determined from the viscosity curves. Gel times are rounded to nearest 5min

Sample	Gel time [min]
9 wt% 325 mM 20°C No Shear	155
12 wt% 325 mM 20°C No Shear	70
12 wt% 400 mM 20°C No Shear	25
12 wt% 325 mM 40°C No Shear	30
12 wt% 325 mM 20°C 1000s ⁻¹	40

reduced. The point where the growth rate is starting to decline, around 70 min, correspond well with the gel time determined from the viscosity in Fig. 11a, listed in Table 1. The gel time is determined based on the intersection of two linear fits of the viscosity data, as demonstrated in Fig. 7. The first linear region is based on the constant viscosity area before the onset of the viscosity increase. The second linear region is estimated based on the region around the inflection point of the curve. The inflection point is determined from the sigmoidal fit of the viscosity data. Table 1 gives an overview of the gel times for different samples, acquired using the method described above.

The cluster size for the lower silica concentration of 9 wt% keeps increasing until the sample starts to gel around 155 min, where the growth rate starts to diminish for this sample as well. Interestingly, the average cluster size for the high silica concentration (12 wt%) starts to level out around 20 nm, whereas the size for the lower silica concentration (9 wt%) continues to increase to a value close to 30 nm. It could be argued that the final cluster sizes are so different due to the large difference in measurement time, with the low silica sample being measured for 160 min, and the high silica sample being measured for 80 min. However, the sample of 12 wt% was measured again after 7 h, at which point the cluster size had only increased to 25 nm, without any change in the fractal dimension. Thus, even with longer waiting times the end products are not the same. It seems that the higher silica concentration, while leading to initially faster aggregation kinetics, also contributes to “locking” the system, limiting the diffusion and thus the maximum size that the aggregates can obtain. The fact that changing the silica concentration alters the end structure was also found by Zhang et al. [33], different silica concentrations over a long period of time, up to two weeks. They found that increasing the silica volume fraction caused the characteristic of the gel formation to change from reaction limited cluster aggregation of a fractal network to a final structure resembling that of a compact solid.

As can be generally seen in Figs. 8, 9, 10 and 11 the measuring times are unequal for the different samples. This is due both to the differences in gel times, as some samples required much longer times to gel, e.g. the 9 wt% sample, and to practical constraints within a limited beamtime.

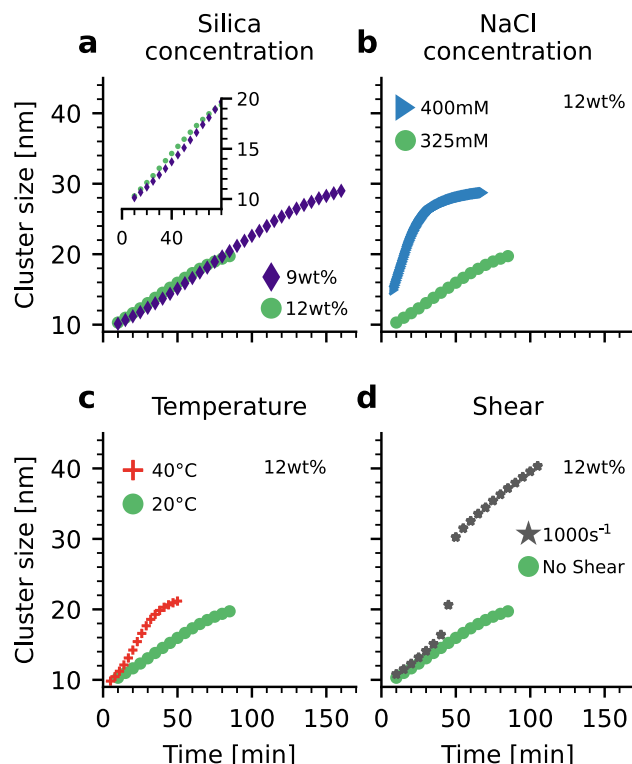
Another parameter extracted from the Beaucage Unified Fit is the fractal dimension. From Fig. 10a it can be seen that for equal times the fractal dimension, α , is always larger for the sample of lower silica concentration; however, the difference is greatest in the first 30 min. This parameter can be used to describe how densely the clusters are packed, and to distinguish between a mass-fractal and surface fractal system. A value around 2.2 is well within the range for a mass-fractal, and also indicates a relatively open structure. From the fractal dimension one can also determine if the aggregation is governed by a diffusion limited cluster aggregation (DLCA) or reaction limited cluster aggregation (RLCA). A fractal dimension between 1.7 and 1.8 indicates DLCA, while values between 1.9 and 2.1 generally describe reaction limited aggregation [34, 35]. Higher values indicate reaction limited aggregation with reorganization [3]. With our values close to 2.2 for all systems, we can conclude that the system is governed by diffusion limited cluster aggregation.

In summary, the silica concentration influences the final cluster sizes, as well as having a large effect on the gel time of the system. Reducing the silica concentration by 3 wt% leads to more than a doubling in the gel time. The reduction in silica concentration also slightly alters the fractal dimension of the final system, making the final gel network more densely packed for the lower silica concentration. The latter effect could be related to the difference in the relative amount of NaCl present in the two situations. The NaCl concentration is the same, but at the lower silica concentration the number of salt ions per silica particle is higher, thus compacting the double layer and creating a tighter network. The same effect, although weak, is observed with increasing salt concentration at the same silica concentration in Fig. 10b.

3.2 NaCl concentration

Increasing the activator in the form of NaCl from 325 mM to 400 mM induced a rapid gel formation in the sample. From Fig. 8b, it can be seen that at high q values (range 0.3 nm^{-1} - 0.7 nm^{-1}) a more prominent bump is visible for the 325 mM NaCl concentration, indicating that more of the smaller structures are present, while they have already been aggregated at the same time by the larger NaCl concentration. In the low- q region, the overlap of the first curve for the 400 mM sample with the 40 min curve for the 325 mM sample is nearly perfect, illustrating the point that the network development for the high NaCl concentration is much more rapid. Beyond this, the 400 mM sample has a further increase in intensity. Interestingly, the 400 mM (12 wt%) sample has some similarities with the 9 wt% (325 mM) sample. Looking at the cluster size in Fig. 9a, b, they end up at almost exactly the same value. The only difference is that the development is more rapid for the 400 mM sample. In addition, at 12 wt% silica fractal dimension for the high NaCl concentration is also slightly larger than at the low concentration. It is, however, still lower than what was obtained at lower silica concentration (9 wt%). Zhang et al. [33] found that varying the activator concentration and type did not influence the final structure of their gel system, but instead only produced an effect on the kinetics of the system. From the measurements we have performed it is not possible to say anything about the structure after long aging times. The measurements performed by Zhang et al. [33] was performed over several weeks. Our data on the other hand suggests that the structures forming in the early stages

Fig. 9 Cluster size as a function of time for five samples. **a** Comparison of two different silica concentrations. 9 wt% and 12 wt% silica, 325 mM NaCl, 20°C and no applied shear. **b** Comparison of two different NaCl concentrations. 325 mM and 400 mM NaCl, 12 wt% silica, 20°C and no applied shear. **c** Comparison of two different temperatures. 20°C and 40°C, 12 wt% silica, 325 mM NaCl and no shear applied. **d** Comparison of different applied shear. No shear and 1000s⁻¹, 12 wt% silica, 325 mM NaCl at 20°C



of aggregation with different activator concentrations are somewhat different, with differences in cluster size and minor changes in the fractal dimension.

A rapid gel time of 25 min is displayed for the 12 wt% system at 400 mM salt in Fig. 11b and listed in Table 1. As this sample was measured for an extended time after gelling occurred, the viscosity increase appears to be much larger compared with the lower salt concentration. It also seems like the rate of increase of the viscosity is reduced by the end of the measurement, as indicated by the slight decrease in the slope of the curve. It is generally known and accepted that a gelling system often show a continuously increasing viscosity over a very long time span. Thus, the higher viscosity is only an effect of the measurement time.

A reduction in gel time as activator concentration is increased has been observed by several others [15–17, 33, 36–38]. The increase in electrolyte concentration causes a screening of the surface charges on the particles, which in turn causes them to approach each other as the electrostatic repulsion is decreased. This leads to aggregation and gel formation in our system. The Debye screening length for the two salt concentrations can be calculated to 0.53 nm and 0.48 nm for 325 mM and 400 mM NaCl, respectively, which is only a decrease of 0.05 nm. Despite this small reduction in screening length between the two NaCl concentrations, a rather large reduction in the gelation time is observed for the increase in NaCl concentration. This disproportionate reduction could indicate that there are other cooperative effects present. The value for CaCl₂ at 5 mM concentration, as employed for the samples shown in Fig. 2, yields a value of 8.6 nm. Despite the screening length being larger for CaCl₂ than for NaCl, instant gelling is observed when mixing with CaCl₂. One possible explanation for this counter-intuitive behavior is the influence of hydration of the cation and silica. At pH values above 9 the silica surface is highly deprotonated and probably has a strong hydration layer. Dissolved monovalent ions like Na⁺ and divalent ions like Ca²⁺ will be surrounded by ordered water, but with the number of water molecules typically being higher for Ca²⁺ than for Na⁺ [39]. Since highly hydrated surfaces tend to show enhanced interaction with strongly hydrated ions, partially due to the polarization of the surrounding water, this could be one reason why we see a stronger gelling effect with CaCl₂. A separate observation is that ion-ion correlation effects arising with divalent counterions are argued to play a significant role in the aggregation and cohesion of silica particles in cement slurries [40]. The ion-ion correlation can cause charge reversal of negative silica, and thus strong attraction. These forces are most prominent at high calcium concentration and at high surface charge densities.

Both increasing the activator concentration and increasing the silica concentration contribute to lowering the gel time. Recalculating the NaCl concentration into weight percent, it can be shown that an increase of only 0.4 wt%, corresponding to a 23 % relative increase in NaCl, leads to a decrease in gel time of 63 %. Measurements for a sample at 9 wt% SiO₂ with the same change from 325 to 400 mM displays nearly the same percent-wise decrease in gel time, with the decrease from 155 to 55 min corresponding to a 64 % reduction. Thus, it seems like for the low silica concentrations in this study, the decrease in gel time due to the same change in salinity is independent

Fig. 10 Fractal dimension as a function of time for five samples. **a** Comparison of two different silica concentrations. 9 wt% and 12 wt% silica, 325 mM NaCl, 20°C and no applied shear. **b** Comparison of two different NaCl concentrations. 325 mM and 400 mM NaCl, 12 wt% silica, 20°C and no applied shear. **c** Comparison of two different temperatures. 20°C and 40°C, 12 wt% silica, 325 mM NaCl and no shear applied. **d** Comparison of different applied shear. No shear and 1000s⁻¹, 12 wt% silica, 325 mM NaCl at 20°C

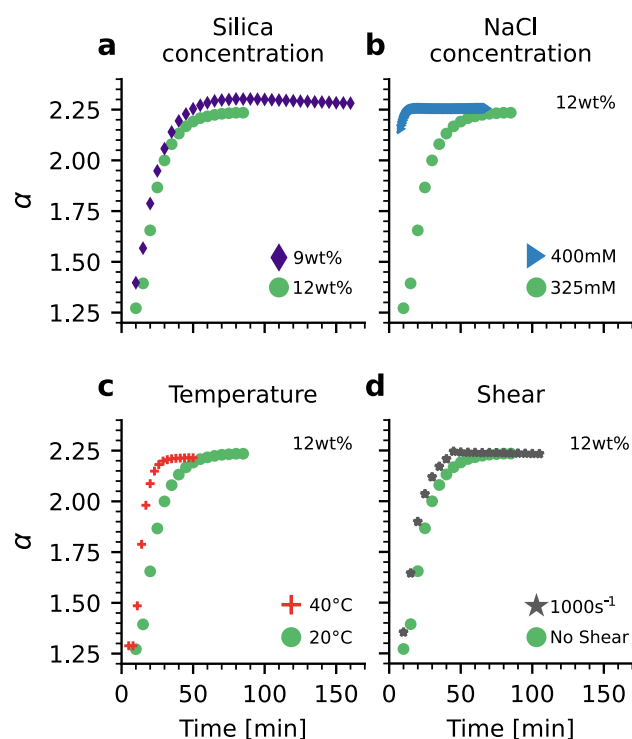
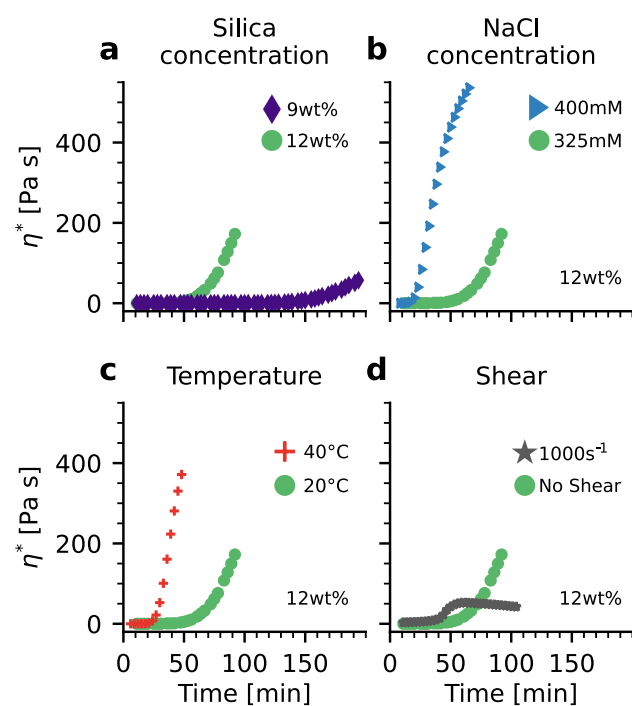


Fig. 11 Complex viscosity, η^* , as a function of time for the different samples. **a** Comparison of two different silica concentrations. 9 wt% and 12 wt% silica, 325 mM NaCl, 20°C and no applied shear. **b** Comparison of two different NaCl concentrations. 325 mM and 400 mM NaCl, 12 wt% silica, 20°C and no applied shear. **c** Comparison of two different temperatures. 20°C and 40°C, 12 wt% silica, 325 mM NaCl and no shear applied. **d** Viscosity, η , of samples with different applied shear. No shear and 1000s⁻¹, 12 wt% silica, 325 mM NaCl at 20°C



of the silica concentration. A scaling behavior of gel times onto a master curve for varying gel times as a function of silica concentration has already been observed by several authors [33, 38, 41, 42]

Concerning the silica concentration, a 3 wt% increase in silica concentration, corresponding to a 33 % relative increase, causes a 56 % decrease in gel time. From this it appears that salinity has a stronger effect on the gel time compared to the silica concentration. A similar trend was found by Pham and Hatzignatiou [17], where it was shown that a 10 wt% increase in activator concentration caused a reduction in gel time of 62 h, while the same change in silica concentration only gave a 13 h reduction.

3.3 Temperature

Looking at Fig. 8c it appears that increasing temperature does not influence the structure except for developing it faster. The scattering curves all have the same shape and would have overlapped if shifted vertically. Note that the first curve for the higher temperature has a higher intensity at low q values and lower intensity at high q values, which is opposite to what was expected. This is due to the measurement being started 5 min after NaCl addition, instead of 10 min as for the lower temperature. Additionally, it takes some time for the temperature of the liquid in the cup to reach 40°C, as it is at room temperature when being transferred into the rheometer.

The fitting parameters show that the cluster size for the 40°C sample starts slightly below the 20°C sample; however, it increases faster and so within the first 10 min the cluster size is larger for the higher temperature (Fig. 9c). Increasing temperature causes an increase of the Brownian motion of the particles, leading to a higher collision frequency, and thereby a more rapid generation of the gel network. The final cluster size is also slightly larger for the high-temperature case, but not as much as induced by higher NaCl or lower silica concentration. The fractal dimension for the high-temperature sample is also larger and increasing faster compared to the low-temperature sample, but with the final fractal dimension being slightly lower. Amiri et al. [35] investigated a similar system of colloidal silica as a function of temperature using a rheological approach. By calculating the fractal dimension based on a relaxation exponent, they found that the fractal dimension decreased with an increase in temperature from 2.48 at 18°C to 2.21 at 35°C. In addition to this, they also observed a large decrease in gelation time with increased temperature, as well as an increase in aggregate size. These changes are consistent with a more open network of larger clusters at higher temperature. A much stronger decrease in fractal dimension obtained through SAXS was found by Wijnen et al. [3] who investigated the effect of temperature on the aging of a potassium water glass. They found that the increased temperature caused a decrease in fractal dimension due to dissolution of silica from the peripheral network combined with a precipitation in the center of the network. On the other hand, other authors have found an increase in the fractal dimension with increasing temperature [4, 43]. Wu et al. [43] found that the fumed silica in dodecane that they studied became denser with an increase in temperature. The restructuring was ascribed to a sliding of the fumed silica along the aggregates surface, stabilizing in a conformation with a lower Gibbs free energy. Although there could be several possible explanations for the lower fractal dimension observed at the higher temperature it is important to stress that the observed difference in our system is very small. However, with longer aging times, or higher temperatures the difference might become more prominent.

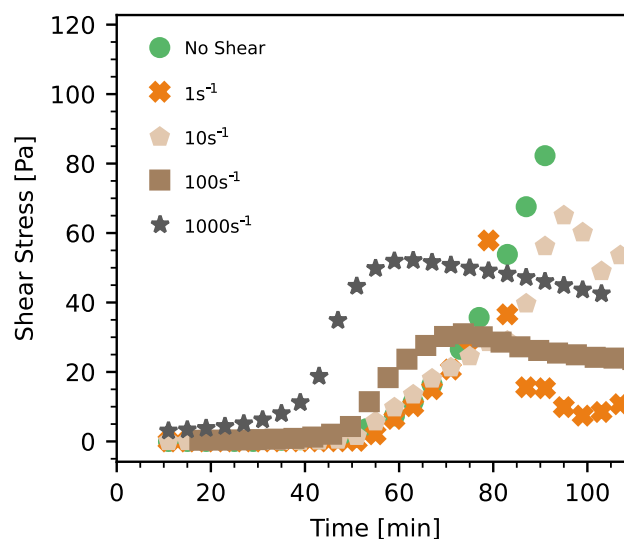
By raising the temperature from 20°C to 40°C, the gel time is reduced to 30 min, as seen by the viscosity increase in Fig. 11c and Table 1. Similarly to the viscosity of the high salinity sample in Fig. 11b, the viscosity for the high temperature is also increasing far beyond the viscosity of the low-temperature sample, which is probably due to the same reasons as for the high salinity case, namely that the sample is measured for some time after it has gelled. Comparing the reduction in gel time with the one induced by increasing the NaCl concentration or the silica concentration we find that an increase from 20°C to 40°C only caused a 57 % decrease in gel time. This is a smaller percent-wise decrease in gel time than the silica and NaCl concentration produced. Thus, ranking the effects of the different parameters on reducing the gel time, the order becomes NaCl > SiO₂ > temperature.

Overall, increasing the temperature does not change the final structure of the gel network significantly on the time scale probed in our experiments. The kinetics are, however, strongly affected and more rapid for the higher temperature.

3.4 Shear

To probe the effect of shear on the structure of the gel, a constant high shear rate of 1000s⁻¹ was applied. From Fig. 8d, it can be seen that the scattering curves initially are overlapping well. As time progresses a radical change occurs for the sample with an applied shear. Approximately between 40 and 50 min there is a transition in the smooth development of the scattering curves. The slope at low q increases and the last part of the curves becomes straight lines, as opposed to flattening out to plateaus. Such an abrupt increase in scattering intensity at low q was also observed by Hanley et al. [44] in their experiments using high shear rate on a colloidal silica. In addition to the abrupt change in scattering intensity, they also observed a peak in viscosity, followed by a rapid decline. These effects were attributed to a densification of the clusters. This argument was supported by their calculation of the fractal dimension of the system which displayed an increase from 1.4 before gelling to 2.4 after the gel point was reached. The rapid decrease in viscosity after reaching a peak value is not observed to the same extent in our system. From Fig. 11d it can be seen that the decline in viscosity (1000s⁻¹ curve) is much slower, however it is still present. The difference could be due to the much higher silica concentrations used in their study. This could also explain the lower shear stress values obtained in our system, as shown in Fig. 12. However, in Fig. 12 the existence of a maximum shear stress that is relatively independent of the shear rate is observed, similar to what Hanley et al. [44] discovered. Later, others have also investigated the effect of shear on the micro-structure of evolving silica gels [45–48].

Fig. 12 Shear stress as a function of time for samples exposed to different shear rates. Samples have 12 wt% SiO₂, 325 mM NaCl and are kept at 20°C



Recently Muzny et al. [45] further investigated the time-dependent behavior of a gel-initiated silica solution subjected to an applied shear. They combined USANS and SANS to cover both the nano- and microscale structures developed in the system. From these investigations it was concluded that a gel network developing under a constant shear is broken at the point which would have corresponded to the gel point, allowing for the clusters to densify and continue to grow, in line with the results obtained by Hanley et al. [44]. From Fig. 10d it can be seen that the fractal dimension in our system is always larger for the sheared sample during the development of the gel, supporting the argument of a densification of clusters. On the other hand, the final fractal dimension for the two systems are quite similar. This could also be an effect of time, as the samples in ref.[45] were measured over a longer time span. We also observe an increase in cluster size close to the gel point for the sheared sample, as seen in Fig. 9d, consistent with the cluster growth found in refs. [44–46]. Some authors have reported anisotropy in sheared samples [47]. Such anisotropies have not been observed in the scattering patterns in this study (see Online Resource, Fig. S1). However, due to the challenges of detecting anisotropies in small length scales, the existence of such anisotropies cannot be excluded as a possibility.

In short, applying a shear to the colloidal silica system causes major changes both structurally and rheologically. The shear produces larger clusters with less connectivity between them preventing the system from forming a gel structure that span the complete volume of the container.

3.5 Magnetic field and particles

At the BM26 beamline at ESRF, silica gels containing various amounts of magnetic microparticles were prepared in capillaries and inserted into the magnetic field at the sample stage. The field strength applied was between 0.1 T and 4 T. We investigated the effect on the silica gel structure of adding magnetic particles and applying a magnetic field, as seen in Figs. 13 and 14. In Fig. 13 it can be seen that the scattering patterns for one sample without and one with 0.5 wt% magnetic microparticles are largely overlapping in the high- q regime, that corresponds to the length scale of individual silica particles. However, at lower q the sample with no magnetic particles have a stronger scattering, indicating that more of the larger clusters are forming at an earlier stage in this sample (cluster size development and fractal dimension plots for these samples can be found in Fig. S2 and Fig. S3 in the Online Resource). Similar measurements with magnetic particle concentrations of 0.1 wt% and 1 wt%, as well as for samples of higher NaCl concentrations with 0.1 wt% and 0.5 wt% display the same tendencies of suppressing scattering at lower q with increasing magnetic particle concentration. The results for 0.1 wt% and 1 wt% at 325 mM can be seen in Fig. 15. Due to the large size of the magnetic microparticles, they displayed settling on the capillary walls, with some chain formation at the lower magnetic fields. Consequently the explanation for the suppression of the cluster growth due to increase in magnetic particle concentration is challenging. Most studies combining colloidal silica with magnetic materials involve the incorporation of, e.g. iron oxide nanoparticles into the structure of the colloidal silica [49, 50].

Fig. 13 Scattering intensity, I , as a function of scattering vector q . Each curve represents a different moment in time, marked by the different colors. Comparison of two different magnetic particle concentrations, 0 wt% and 0.5 wt% with a silica concentration of 12 wt%, NaCl concentration of 325 mM, temperature 20°C at a magnetic field of 0.1 T

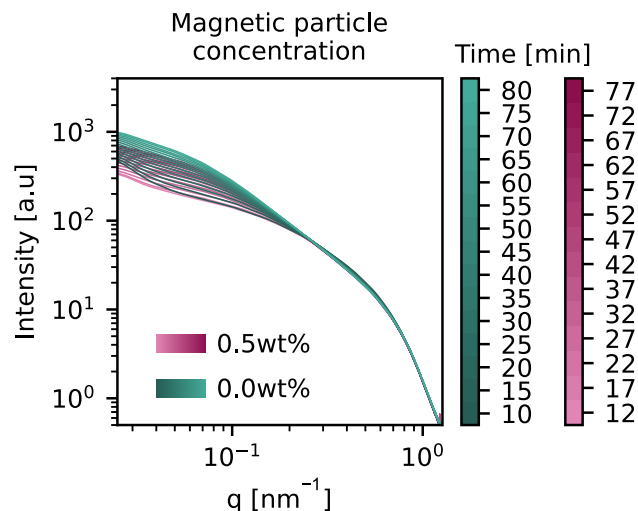
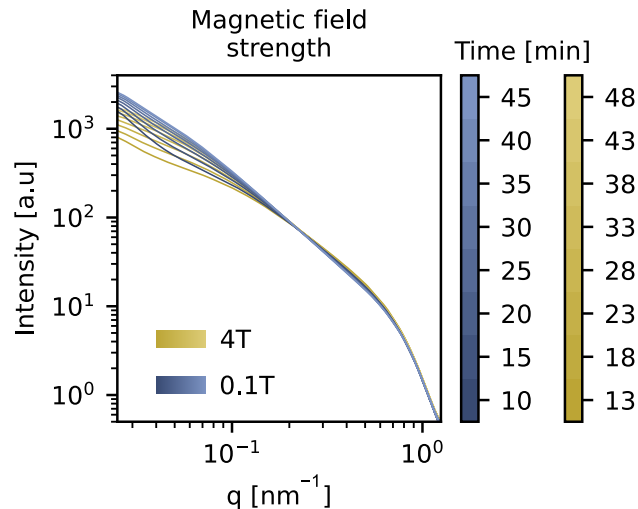


Fig. 14 Scattering intensity, I , as a function of scattering vector q . Each curve represents a different moment in time, marked by the different colors. Comparison of two different magnetic field strengths, 0.1 T and 4 T with a silica concentration of 12 wt%, NaCl concentration of 400 mM, temperature 20°C and magnetic particle concentration of 1 wt%



Similarly, two samples were measured at different magnetic field strengths of 0.1 T and 4 T. The results in Fig. 14 show a similar tendency as that of increasing the magnetic particle concentration. Increasing the magnetic field strength appears to suppress the larger cluster formation, seen as a lower scattering intensity at low- q values. A depression of cluster growth of a silica gel with high magnetic field was also found by Sasahara et al. [51], who discovered that applying a 6 T magnetic field reduced the viscosity the silica solution. This reduction in viscosity was attributed to a possible reduction in the interactions between particles with OH groups due to the magnetic field. It was also found that an intermediate species of the sodium silicate solution reacted faster at the high magnetic field, possibly leading to the decrease in particle sizes, as the magnetic field promotes hydration around microgels [51]. Another investigation of silica gel formation under magnetic field found that anisotropic gel networks were produced [52]. From the scattering patterns of the silica gel exposed to high magnetic field during gelling, we have not observed any anisotropy reflecting an ordering of the gel network.

In contrary to what we are observing for the present system, magnetic fields have been shown to enhance the aggregation and precipitation of silica in brackish water distribution systems for irrigation. This process involves the use of a permanent magnetic field placed on a pipeline. It is believed that the reduction of silica due to the influence of a magnetic field is through a suppression of the electrical double layer, causing silica to aggregate and precipitate, resulting in its filtering out before reaching the drip irrigation lines [53]. On the other hand, these observations are on a larger scale than our study. It is possible that the magnetic field inhibits the early cluster formation of colloidal silica, while enhancing it once it has passed a threshold in aggregate size.

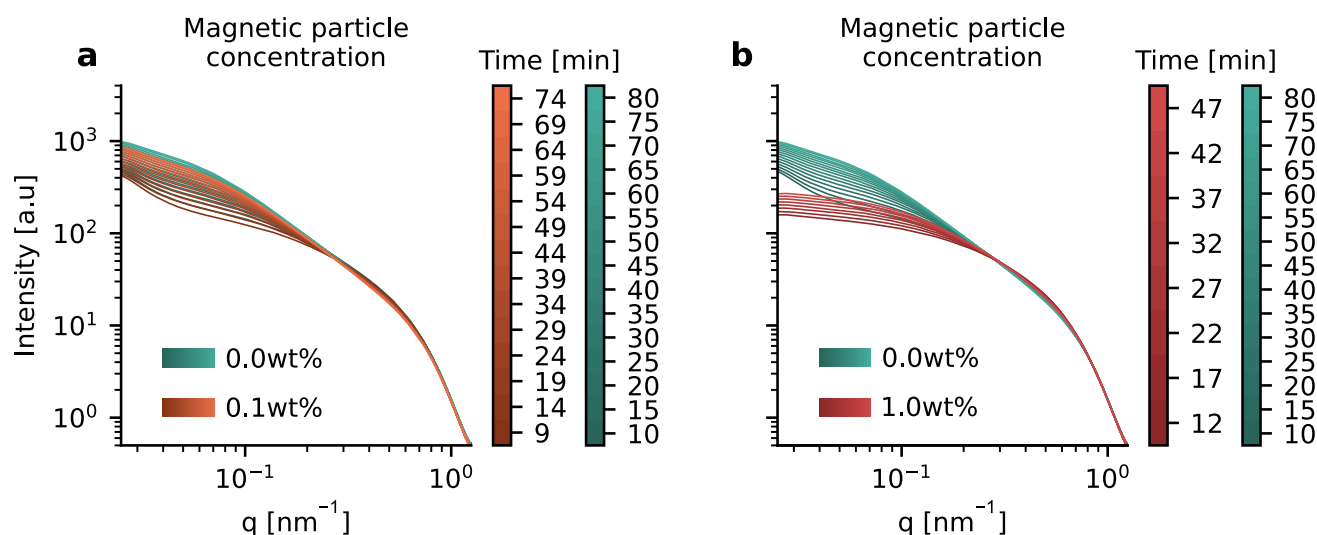


Fig. 15 Scattering intensity, I , as a function of scattering vector q . Each curve represents a different moment in time, marked by the different colors. **a, b** Comparison of two different magnetic particle concentrations. 12 wt% silica, 325 mM NaCl, 20°C at 0.1 T

4 Conclusion

Both macroscopic and microscopic properties of a silica colloidal gel system have been investigated simultaneously by use of small angle X-ray scattering and rheology. We found that the activator concentration in form of NaCl had the strongest effect on gel time, followed by the silica concentration and lastly the temperature. Both the silica concentration and the NaCl concentration have some effect on the final structure of the gel network, producing larger clusters for lower silica concentrations and higher NaCl concentrations, and increasing the fractal dimension, leading to denser gel networks. Increasing temperature on the other hand does not seem to impose large changes in the gel structure. An applied shear causes major structural changes in the network. The developing network is broken while forming, allowing the clusters to grow more. Additionally, macroscopically a gel is not formed, but a viscous fluid. Lastly, applying a magnetic field, or adding magnetic microparticles to the gelling colloidal silica appears to be suppressing larger cluster formation. Due to the limited literature on the topic of magnetic field effect on silica gel systems, these effects should be further investigated.

Supplementary Information The online version contains supplementary material available at <https://doi.org/10.1140/epjs/s11734-024-01250-y>.

Acknowledgements This work was supported by the Research Council of Norway under the project “Nanofluids for IOR and Tracer Technology”—PETROMAKS2, project number 280643. We acknowledge Diamond Light Source and the European Synchrotron Radiation Facility (ESRF) for provision of synchrotron radiation facilities. We would like to thank Andy Smith for the assistance in using beamline I22, and Martin Rosenthal for the assistance in using beamline BM26. In addition, we would like to thank the XMaS beamline at the ESRF for the use of the superconducting magnet lent to BM26 for our experiment. We also acknowledge Nouryon for providing the samples for our investigation. *This work benefited from the use of the SasView application, originally developed under NSF award DMR-0520547. SasView contains code developed with funding from the European Union’s Horizon 2020 research and innovation programme under the SINE2020 project, grant agreement No 654000.*

Author contribution statement

Konstane Kvaem Seljelid, Jon Otto Fossum, Kenneth Dahl Knudsen and Ingebret Fjelde contributed to the study conception and design. Material preparation and data collection were performed by Konstane Kvaem Seljelid, Osvaldo Trigueiro Neto, Andrew Ndubuisi Akanno, Bruno Telli Ceccato, Rini Padinjakkara Ravindranathan, Namrah Azmi and Leide P. Cavalcanti. Analysis were performed by Konstane Kvaem Seljelid, Jon Otto Fossum and Kenneth Dahl Knudsen. The first draft of the manuscript was written by Konstane Kvaem Seljelid and all authors commented on previous versions of the manuscript. All authors read and approved the final manuscript.

Funding Open access funding provided by NTNU Norwegian University of Science and Technology (incl St. Olavs Hospital - Trondheim University Hospital).

Data availability statement Data sets generated during the current study are available from the corresponding author on reasonable request.

Declarations

Conflict of interest The authors have no financial or proprietary interests in any material discussed in this article.

Open Access This article is licensed under a Creative Commons Attribution 4.0 International License, which permits use, sharing, adaptation, distribution and reproduction in any medium or format, as long as you give appropriate credit to the original author(s) and the source, provide a link to the Creative Commons licence, and indicate if changes were made. The images or other third party material in this article are included in the article's Creative Commons licence, unless indicated otherwise in a credit line to the material. If material is not included in the article's Creative Commons licence and your intended use is not permitted by statutory regulation or exceeds the permitted use, you will need to obtain permission directly from the copyright holder. To view a copy of this licence, visit <http://creativecommons.org/licenses/by/4.0/>.

References

1. K. Hans Wedepohl, The composition of the continental crust. *Geochim. Cosmochim. Acta* **59**(7), 1217–1232 (1995). [https://doi.org/10.1016/0016-7037\(95\)00038-2](https://doi.org/10.1016/0016-7037(95)00038-2)
2. J.B. Peri, A.L.J. Hensley, The surface structure of silica gel. *J. Phys. Chem.* **72**(8), 2926–2933 (1968). <https://doi.org/10.1021/j100854a041>
3. P.W.J.G. Wijnen, T.P.M. Beelen, K.P.J. Rummens, H.C.P.L. Saeijs, R.A. Van Santen, Silica gel from water glass: a SAXS study of the formation and ageing of fractal aggregates. *J. Appl. Crystallogr.* **24**(5), 759–764 (1991). <https://doi.org/10.1107/S0021889891000924>
4. M. Chen, W.B. Russel, Characteristics of flocculated silica dispersions. *J. Colloid Interface Sci.* **141**(2), 564–577 (1991). [https://doi.org/10.1016/0021-9797\(91\)90353-A](https://doi.org/10.1016/0021-9797(91)90353-A)
5. A.S. Zackrisson, J.S. Pedersen, J. Bergenholtz, A small-angle X-ray scattering study of aggregation and gelation of colloidal silica. *Colloids Surf. A* **315**(1–3), 23–30 (2008). <https://doi.org/10.1016/j.colsurfa.2007.07.004>
6. K. Okazaki, M. Kawaguchi, Influence of Monovalent Electrolytes on Rheological Properties of Gelled Colloidal Silica Suspensions. *Journal of Dispersion Science and Technology* **29**(1), 77–82 (2008). <https://doi.org/10.1080/01932690701688425>. Publisher: Taylor & Francis _eprint: 10.1080/01932690701688425
7. M.B. Gordon, C.J. Kloxin, N.J. Wagner, The rheology and microstructure of an aging thermoreversible colloidal gel. *J. Rheol.* **61**(1), 23–34 (2017). <https://doi.org/10.1122/1.4966039>
8. G.E. Gimenes, E. Bouchaud, Flow and fracture near the sol-gel transition of silica nanoparticle suspensions. *Soft Matter* **14**(39), 8036–8043 (2018). <https://doi.org/10.1039/C8SM01247D>
9. G. Hu, S. Jin, K. Liu, Structure-Directing Effect on Silica Nanoparticle Growth in Sodium Silicate Solutions through Small-Angle X-ray Scattering. *The Journal of Physical Chemistry C* **127**(22), 10585–10593 (2023). <https://doi.org/10.1021/acs.jpcc.3c01112>
10. K.C. Ng, H.T. Chua, C.Y. Chung, C.H. Loke, T. Kashiwagi, A. Akisawa, B.B. Saha, Experimental investigation of the silica gel-water adsorption isotherm characteristics. *Appl. Therm. Eng.* **21**(16), 1631–1642 (2001). [https://doi.org/10.1016/S1359-4311\(01\)00039-4](https://doi.org/10.1016/S1359-4311(01)00039-4)
11. C.A. Grande, D.G.B. Morence, A.M. Bouzga, K.A. Andreassen, Silica Gel as a Selective Adsorbent for Biogas Drying and Upgrading. *Industrial & Engineering Chemistry Research* **59**(21), 10142–10149 (2020). <https://doi.org/10.1021/acs.iecr.0c00949>
12. U. Schloßmacher, H.C. Schröder, X. Wang, Q. Feng, B. Diehl-Seifert, S. Neumann, A. Trautwein, W.E.G. Müller, Alginate/silica composite hydrogel as a potential morphogenetically active scaffold for three-dimensional tissue engineering. *RSC Adv.* **3**(28), 11185–11194 (2013). <https://doi.org/10.1039/C3RA23341C>. (Publisher: The Royal Society of Chemistry)
13. R. Ravichandran, D. Sundaramurthi, S. Gandhi, S. Sethuraman, U.M. Krishnan, Bioinspired hybrid mesoporous silica-gelatin sandwich construct for bone tissue engineering. *Microporous Mesoporous Mater.* **187**, 53–62 (2014). <https://doi.org/10.1016/j.micromeso.2013.12.018>
14. S. Liu, W.K. Ott, Sodium silicate applications in oil, gas & geothermal well operations. *J. Petrol. Sci. Eng.* **195**, 107693 (2020). <https://doi.org/10.1016/j.petrol.2020.107693>
15. C.O. Metin, K.M. Rankin, Q.P. Nguyen, Phase behavior and rheological characterization of silica nanoparticle gel. *Appl. Nanosci.* **4**(1), 93–101 (2014). <https://doi.org/10.1007/s13204-012-0168-7>
16. D.G. Hatzignatiou, R. Askarinezhad, N.H. Giske, A. Stavland, Laboratory Testing of Environmentally Friendly Sodium Silicate Systems for Water Management Through Conformance Control. *SPE Production & Operations* **31**(04), 337–350 (2016). <https://doi.org/10.2118/173853-PA>

17. L.T. Pham, D.G. Hatzignatiou, Rheological evaluation of a sodium silicate gel system for water management in mature, naturally-fractured oilfields. *J. Petrol. Sci. Eng.* **138**, 218–233 (2016). <https://doi.org/10.1016/j.petrol.2015.11.039>
18. A.-C.J.H. Johnsson, M.C. Camerani, Z. Abbas, Combined Electrospray-SMPS and SR-SAXS Investigation of Colloidal Silica Aggregation. Part I. Influence of Starting Material on Gel Morphology. *The Journal of Physical Chemistry B* **115**(5), 765–775 (2011) <https://doi.org/10.1021/jp1057995>
19. A.-C.J.H. Johnsson, M.C. Camerani, Z. Abbas, Combined Electrospray-Scanning Mobility Particle Sizer (ES-SMPS) and Time-Resolved Synchrotron Radiation-Small-Angle X-ray Scattering (SR-SAXS) Investigation of Colloidal Silica Aggregation. Part II. Influence of Aggregation Initiator on Gel Stability. *The Journal of Physical Chemistry B* **115**(31), 9547–9555 (2011) <https://doi.org/10.1021/jp2032753>. Publisher: American Chemical Society
20. K. Whitcomb, Determining the linear viscoelastic region in oscillatory measurements. Application note, TA Instruments. <https://www.tainstruments.com/pdf/literature/RH107.pdf>
21. M. Basham, J. Filik, M.T. Wharmby, P.C.Y. Chang, B. El Kassaby, M. Gerring, J. Aishima, K. Levik, B.C.A. Pulford, I. Sikharulidze, D. Sneddon, M. Webber, S.S. Dhesi, F. Maccherozzi, O. Svensson, S. Brockhauser, G. Náráy, A.W. Ashton, Data Analysis Workbench (DAWN). *J. Synchrotron Radiat.* **22**(3), 853–858 (2015). <https://doi.org/10.1107/S1600577515002283>
22. J. Filik, A.W. Ashton, P.C.Y. Chang, P.A. Chater, S.J. Day, M. Drakopoulos, M.W. Gerring, M.L. Hart, O.V. Magdysyuk, S. Michalik, A. Smith, C.C. Tang, N.J. Terrill, M.T. Wharmby, H. Wilhelm, Processing two-dimensional X-ray diffraction and small-angle scattering data in DAWN 2. *J. Appl. Crystallogr.* **50**(3), 959–966 (2017). <https://doi.org/10.1107/S1600576717004708>
23. V. Dyadkin, P. Pattison, V. Dmitriev, D. Chernyshov, A new multipurpose diffractometer PILATUS@SNBL. *J. Synchrotron Radiat.* **23**(3), 825–829 (2016). <https://doi.org/10.1107/S1600577516002411>. (Number: 3 Publisher: International Union of Crystallography)
24. S. Jarratt, XMaS Beamline - Sample Environments - Magnetic Fields. https://warwick.ac.uk/fac/cross_fac/xmas/xmasbeamline/sample_environments/magnetic_fields (Accessed: 2023-12-18)
25. G. Beaucage, Approximations leading to a unified exponential/power-law approach to small-angle scattering. *J. Appl. Crystallogr.* **28**(6), 717–728 (1995)
26. G. Beaucage, D.W. Schaefer, Structural studies of complex systems using small-angle scattering: a unified Guinier/power-law approach. *J. Non-Cryst. Solids* **172–174**, 797–805 (1994). [https://doi.org/10.1016/0022-3093\(94\)90581-9](https://doi.org/10.1016/0022-3093(94)90581-9)
27. G. Beaucage, Small-angle scattering from polymeric mass fractals of arbitrary mass-fractal dimension. *J. Appl. Crystallogr.* **29**(2), 134–146 (1996)
28. G. Beaucage, H.K. Kammler, S.E. Pratsinis, Particle size distributions from small-angle scattering using global scattering functions. *J. Appl. Crystallogr.* **37**(4), 523–535 (2004). <https://doi.org/10.1107/S0021889804008969>
29. G. Beaucage, Determination of branch fraction and minimum dimension of mass-fractal aggregates. *Phys. Rev. E* **70**(3), 031401 (2004). <https://doi.org/10.1103/PhysRevE.70.031401>
30. O. Kuzminskaya, S. Riemer, R. Dalglish, L. Almásy, I. Hoffmann, M. Gradzielski, Structure and Phase Behavior of Interpolyelectrolyte Complexes of PDADMAC and Hydrophobically Modified PAA (HM-PAA). *Macromol. Chem. Phys.* **224**(1), 2200276 (2023). <https://doi.org/10.1002/macp.202200276>
31. E.M. Anitas, Small-Angle Scattering from Mass and Surface Fractals. In: López-Ruiz, R. (ed.) Complexity in Biological and Physical Systems - Bifurcations, Solitons And Fractals. InTech, ??? (2018). <https://doi.org/10.5772/intechopen.70870>
32. M. Doucet, J. Cho, G. Alina, J. Bakker, W. Bouwman, P. Butler, K. Campbell, M. Gonzales, R. Heenan, A. Jackson, P. Juhas, S. King, P. Kienzle, J. Krzywon, A. Markvardsen, T. Nielsen, L. O'Driscoll, W.R.F.L. Potrzebowski, T. Richter, P. Rozycko, A. Washington, Sasview version 5.0.5 (2022)
33. L. Zhang, A. Mikhailovskaya, D. Constantin, G. Foffi, J. Tavecchi, J. Schmitt, F. Muller, C. Rochas, N. Wang, D. Langevin, A. Salonen, Varying the counter ion changes the kinetics, but not the final structure of colloidal gels. *J. Colloid Interface Sci.* **463**, 137–144 (2016). <https://doi.org/10.1016/j.jcis.2015.10.046>
34. S. Jungblut, J.-O. Joswig, A. Eychemüller, Diffusion- and reaction-limited cluster aggregation revisited. *Phys. Chem. Chem. Phys.* **21**(10), 5723–5729 (2019). <https://doi.org/10.1039/C9CP00549H>. (Publisher: Royal Society of Chemistry)
35. A. Amiri, G. Øye, J. Sjöblom, Temperature and pressure effects on stability and gelation properties of silica suspensions. *Colloids Surf. A* **378**(1), 14–21 (2011). <https://doi.org/10.1016/j.colsurfa.2011.01.048>
36. D.G. Hatzignatiou, N.H. Giske, D. Strand, Water-soluble silicate gelants: Comparison and screening for conformance control in carbonate naturally fractured reservoirs. *J. Non-Cryst. Solids* **479**, 72–81 (2018). <https://doi.org/10.1016/j.jnoncrysol.2017.10.024>
37. D.G. Hatzignatiou, N.H. Giske, Sodium silicate gelants for water management in naturally fractured hydrocarbon carbonate formations. *Chem. Eng. Res. Des.* **132**, 40–56 (2018). <https://doi.org/10.1016/j.cherd.2017.11.041>
38. X.J. Cao, H.Z. Cummins, J.F. Morris, Structural and rheological evolution of silica nanoparticle gels. *Soft Matter* **6**(21), 5425 (2010). <https://doi.org/10.1039/c0sm00433b>
39. C. Sögaard, K. Kolman, M. Christensson, A.B. Otyakmaz, Z. Abbas, Hofmeister effects in the gelling of silica nanoparticles in mixed salt solutions. *Colloids Surf. A* **611**, 125872 (2021)
40. B. Jönsson, A. Nonat, C. Labbez, B. Cabane, H. Wennerström, Controlling the cohesion of cement paste. *Langmuir* **21**(20), 9211–9221 (2005)

41. P. Sandkühler, J. Sefcik, M. Morbidelli, Scaling of the Kinetics of Slow Aggregation and Gel Formation for a Fluorinated Polymer Colloid. *Langmuir* **21**(5), 2062–2077 (2005). <https://doi.org/10.1021/la048055s>. (Publisher: American Chemical Society)
42. H. Wu, J.-J. Xie, M. Morbidelli, Kinetics of colloidal gelation and scaling of the gelation point. *Soft Matter* **9**, 4437–4443 (2013). <https://doi.org/10.1039/C3SM00117B>
43. X.-J. Wu, Y. Wang, W. Yang, B.-H. Xie, M.-B. Yang, W. Dan, A rheological study on temperature dependent microstructural changes of fumed silica gels in dodecane. *Soft Matter* **8**(40), 10457–10463 (2012). <https://doi.org/10.1039/C2SM25668A>. (Publisher: Royal Society of Chemistry)
44. H.J.M. Hanley, C.D. Muzny, B.D. Butler, G.C. Straty, J. Bartlett, E. Drabarek, Shear-induced restructuring of concentrated colloidal silica gels. *J. Phys.: Condens. Matter* **11**(6), 1369–1380 (1999). <https://doi.org/10.1088/0953-8984/11/6/003>
45. C. Muzny, L. De Campo, A. Sokolova, C.J. Garvey, C. Rehm, H. Hanley, Shear influence on colloidal cluster growth: a SANS and USANS study. *J. Appl. Crystallogr.* **56**(5), 1371–1380 (2023). <https://doi.org/10.1107/S1600576723006726>
46. L. Campo, C.J. Garvey, C.D. Muzny, C. Rehm, H.J.M. Hanley, Micron-scale restructuring of gelling silica subjected to shear. *J. Colloid Interface Sci.* **533**, 136–143 (2019). <https://doi.org/10.1016/j.jcis.2018.08.024>
47. H. Hoekstra, J. Mewis, T. Narayanan, J. Vermant, Multi Length Scale Analysis of the Microstructure in Sticky Sphere Dispersions during Shear Flow. *Langmuir* **21**(24), 11017–11025 (2005). <https://doi.org/10.1021/la051488q>. (Publisher: American Chemical Society)
48. C.D. Muzny, B.D. Butler, H.J.M. Hanley, M. Agamalian, An ultra-small-angle neutron scattering study of the restructuring of sheared colloidal silica gels. *J. Phys.: Condens. Matter* **11**(26), 295–298 (1999). <https://doi.org/10.1088/0953-8984/11/26/101>
49. Q. Liu, J. Zhang, W. Xia, H. Gu, Magnetic field enhanced cell uptake efficiency of magnetic silica mesoporous nanoparticles. *Nanoscale* **4**(11), 3415–3421 (2012). <https://doi.org/10.1039/C2NR30352C>. (Publisher: Royal Society of Chemistry)
50. L. Wan, H. Song, X. Chen, Y. Zhang, Q. Yue, P. Pan, J. Su, A.A. Elzatahry, Y. Deng, A Magnetic-Field Guided Interface Coassembly Approach to Magnetic Mesoporous Silica Nanochains for Osteoclast-Targeted Inhibition and Heterogeneous Nanocatalysis. *Adv. Mater.* **30**(25), 1707515 (2018). <https://doi.org/10.1002/adma.201707515>
51. S. Sasahara, K. Kaida, S. Ozeki, Magnetic Field Effects on Silica Gel Evolution from Aqueous Silicate Solutions. *Chem. Lett.* (2016). <https://doi.org/10.1246/cl.160499>. (Publisher: The Chemical Society of Japan)
52. A. Mori, T. Kaito, H. Furukawa, Structural anisotropy of silica hydrogels prepared under magnetic field. *Mater. Lett.* **62**(19), 3459–3461 (2008). <https://doi.org/10.1016/j.matlet.2008.02.080>
53. Z. Liu, M. Di Luccio, S. García, J. Puig-Bargués, X. Zhao, A. Trueba, T. Muhammad, Y. Xiao, Y. Li, Effect of magnetic field on calcium - silica fouling and interactions in brackish water distribution systems. *Sci. Total Environ.* **798**, 148900 (2021). <https://doi.org/10.1016/j.scitotenv.2021.148900>